Design Optimisation and Global Sensitivity Analysis of a Carnot Battery Towards Integration in a Data Centre under Techno-Economic Uncertainties

A. Laterre*
Institute of Mechanics, Materials and Civil Engineering
Université catholique de Louvain, Louvain-la-Neuve, Belgium
&
Department of Mechanical and Aerospace Engineering
Université de Liège, Liège, Belgium
e–mail* antoine.laterre@uclouvain.be

O. Dumont, V. Lemort
Department of Mechanical and Aerospace Engineering
Université de Liège, Liège, Belgium

F. Contino
Institute of Mechanics, Materials and Civil Engineering
Université catholique de Louvain, Louvain-la-Neuve, Belgium

ABSTRACT

Carnot batteries are quickly-developing technologies that use heat pumps and heat engines to charge and discharge a thermal storage. Although they have multi-scale and multi-application potential, it is still unclear where and how they should be deployed to compete with other storage systems, such as electro-chemical batteries or power-to-X. In this work, we perform the techno-economic optimisation of a small-scale Carnot battery (less than 100 kW) based on the Rankine cycle. This Carnot battery is designed for a real data centre that would be coupled to photovoltaic panels. The main motivation for this integration scenario is the recovery of the cooling water (at 24 °C) from the data centre when charging the system, as this increases the storage electrical efficiency while reducing the data centre energy consumption. This paper first presents the optimisation of two objectives: the minimisation of the data centre Levelized Cost Of Electricity (LCOE) and the maximisation of its Self-Sufficiency Ratio (SSR). For each evaluated design, the two objectives were calculated by performing annual simulations using a thermo-economic model with an hourly resolution including the actual operating conditions of the data centre. Then, the paper describes the impact of the uncertainties of the system parameters on its techno-economic performance. This impact is assessed by a global sensitivity analysis obtained with Polynomial Chaos Expansion. Optimisation results show that there is a clear trade-off between designs that minimise the LCOE and maximise the SSR. They also show that, thanks to the Carnot battery, the data centre can increase its SSR up to 48.5% with a lower LCOE than in the current infrastructure, and while maintaining a similar uncertainty range. The global sensitivity analysis finally suggests that the uncertainties related to the capital and operational costs of the Carnot battery drive the uncertainty on the Levelized Cost Of Storage. Future studies will focus on reducing the uncertainty on the critical parameters.

KEYWORDS

Carnot Battery, Data Centre, Global Sensitivity Analysis, Multi-Objectives Optimisation, Levelized Cost Of Storage, Annual Simulations

* Corresponding author

INTRODUCTION

Electrical Energy Storage (EES) is recognised as a key driver in the transition to intermittent and non-dispatchable renewable energy sources (e.g. wind, solar), as it can bridge the gap between the production and the demand [1]. In this context, finding cost-effective EES systems has become essential. At the same time, sector coupling (i.e. coupling different energy producing and consuming sectors) is perceived as a way to reduce the stress on the required amount of EES while increasing the flexibility and efficiency of energy systems [2]. From this perspective, Carnot batteries (CB), a rapidly developing group of technologies, turn out to be an interesting flexibility option combining energy storage and coupling between electrical and thermal systems [3].

Overview of Carnot batteries

Carnot batteries store energy under the form of heat in thermal energy storage systems. In most implementations, CB are charged with different possible heat pump technologies (HP), and to lesser extent with resistive heaters (RH). They are then discharged with heat engines (HE) that produce electricity [4]. Most HE technologies are either based on the closed Brayton cycle, or on the (organic) Rankine cycle [4]. The main advantages of CB are the possible heat coupling at low or high temperature during the charge or discharge process [5], low expected investment costs and low environmental footprint [4]. Indeed, most concepts propose to store heat in cheap and abundant materials, such as rock, water or molten salts [4], [6].
Although it is possible to imagine a multitude of thermal integration scenarios, it is still unclear where and how could CB compete with other EES technologies, such as chemical batteries [7] or power-to-X [8]. More specifically, techno-economic analyses of low to medium-scale CB (i.e. < 1 MW) are really lacking to initiate their commercial development [4], [6].

Aims of this study

In this work, the techno-economic potential of integrating a CB based on the Rankine cycle in a real 100 kW data centre is investigated. The motivation for this integration scenario is the recovery of the low-grade waste heat (24 °C) from the cooling system when charging the CB, and the reduction of energy consumption dedicated to chilling. To illustrate some typical operating conditions, a photovoltaic array (PV) is installed to support the data centre. Using design optimisation, the goal is to identify CB designs that can maximise the Self-Sufficiency Ratio (SSR) of the data centre, which represents its independence from the grid, while minimising its Levelized Cost Of Electricity (LCOE).
This paper first presents the model of the CB, the PV array and the data centre, followed by the description of the annual data associated with this integration scenario. These data are used to account for performance degradation under off-design conditions and for operational constraints (e.g. PV production, heat source availability, …) when simulating the system. The optimisation algorithm is then briefly discussed. As designing such system is subject to large parameter uncertainty (i.e. CB's have a low Technology Readiness Level [1]), uncertainties related to investment costs and technology performance, as well as those related to meteorological conditions and power consumption, are then introduced. To assess their overall effect on the LCOE, Polynomial Chaos Expansion, the method used to quantify the global uncertainty, is finally explained.

MODEL AND METHOD

In this section, the system model and the corresponding annual data are first presented. The optimisation criteria and the economic considerations are then introduced. Thereafter, the uncertainties characterising the techno-economic parameters of the model are discussed, followed

by a brief description of the method used to propagate the formers and to quantify their effect on the model outputs.

Case study

The integration of a Carnot battery supported by a PV array in the UCLouvain data centre is considered (see Fig. 1). The corresponding climate and demand data are introduced in *Climate and system data*. When the PV array complies with the data centre power demand, excess electricity is stored under the form of heat in the CB, using either a vapour compression HP, either a resistive heater, or both. In HP mode, the evaporator extracts heat from the cooling water. When the PV electricity fails to meet the demand, the CB is discharged with a heat engine based on an organic Rankine cycle. Its heat sink is the cooling water, and the latter is cooled down with the already existing dry cooler. A grid support is also available. All these sub-systems are further discussed below. The full power management strategy is detailed Fig. A1 in *APPENDICES*.

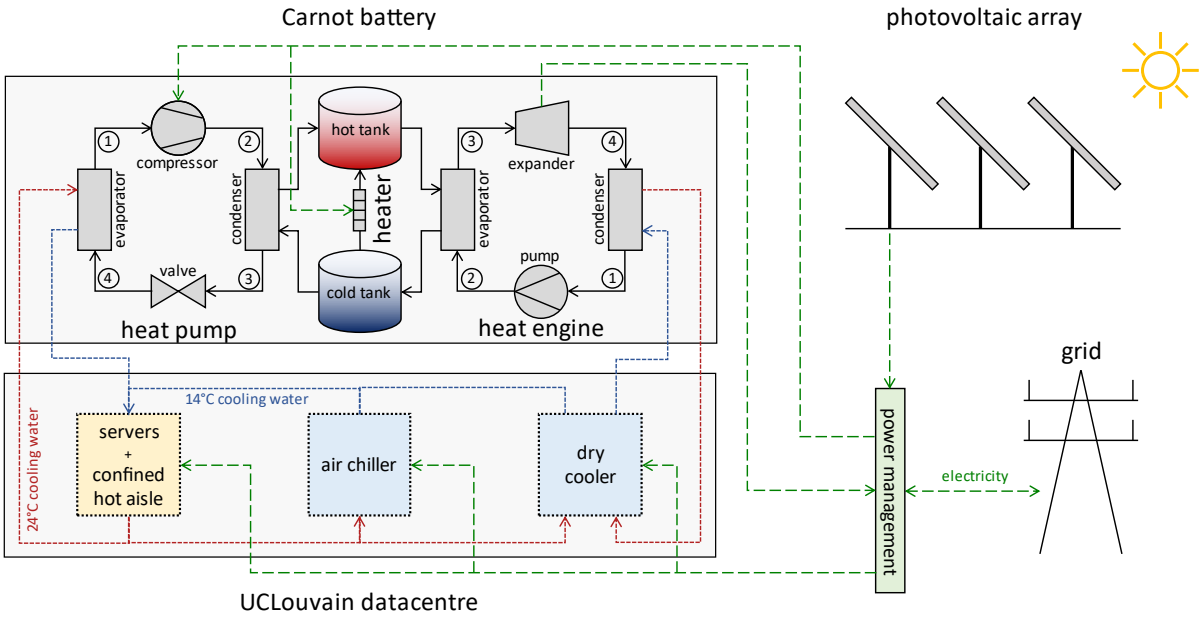

Figure 1. Integration of a CB in the UCLouvain data centre. In HP mode, the evaporator extracts heat from the cooling water. In HE mode, the condenser heat sink is the cooling water.

The UCLouvain data centre is of the hot confined aisle type. The hot air produced by the servers is trapped in an aisle and expelled from it through a chilled water-cooling system. Currently, the water temperature on the hot side $T_{\text{cooling}}^{\text{hot}}$ is about 24 °C. This water is cooled down to 14 °C with a dry cooler when the external temperature is below 12 °C, or with an air chiller. The power consumption of the air chiller and of the dry cooler are unfortunately not available and data reconstruction is therefore employed.

The chiller coefficient of performance (COP) is derived as a fraction $\eta_{\text{chiller}}^{\text{Carnot}}$ of the Carnot COP:

$$\text{COP}_{\text{chiller}} = \frac{Q_{\text{chiller}}^{\text{cold}}}{P_{\text{chiller}}} = \eta_{\text{chiller}}^{\text{Carnot}} \cdot \text{COP}^{\text{Carnot}}\,, \tag{1}$$

where $Q_{\text{chiller}}^{\text{cold}}$ and P_{chiller} are the chiller cooling power and its electrical power respectively. $\text{COP}^{\text{Carnot}}$ is derived based on the temperatures of the cooling water and the ambient air. The value of $\eta_{\text{chiller}}^{\text{Carnot}}$ is given in Tab. A1, in *APPENDICES*.

The power consumption of the dry cooler is assumed to be negligible compared to that of the chiller. This assumption is realistic as the specific power consumption of dry coolers (i.e. inverse of COP, in $[kW_{el}/kW_{th}]$) typically ranges from 0.012 to 0.091 (i.e. COP equivalent ranging from 11 to 81), which is much more efficient than chillers [9].

Thermodynamic model

In this work, all thermodynamic quantities are obtained using `CoolProp` [10].

Charging system: heat pump and resistive heater. The charging system of the CB relies on two components: a vapour compression HP, which uses the hot cooling water as heat source, and a RH, which is used in addition to the HP when the latter reaches its maximum power output. The motivation for this thermal integration [5] is twofold: when charging the CB, the HP recovers the low-grade waste heat (i.e. $T_{\mathrm{cooling}}^{\mathrm{hot}}$ is only 24 °C) and it reduces the chiller power consumption, as the HP does the cooling work for it.

The HP is modelled with its thermodynamic cycle. First, the working fluid evaporates and is super-heated in the low-pressure heat exchanger (HEX) where it absorbs the waste heat from the cooling water. Its exit temperature is obtained with the pinch-point $\Delta T_{\mathrm{pinch}}$ model. This approach is motivated by the lack of knowledge regarding the heat transfer development and by its low computational complexity. It has been used in several other studies [7], [11], [12]. The pressure losses $\Delta p_{\mathrm{hp,ev}}$ are also taken into account.

The fluid pressure is then increased in a volumetric compressor. So far, most authors have used constant efficiency models when optimising the design of CBs [7], [11], [12]. Here, performance degradation in off-design conditions is taken into-account using a simplified version of the semi-empirical model proposed and validated by Lemort [13]. The simplification is introduced to lump the eight losses parameters (accounting for the internal leakages, supply pressure drops, heat losses and friction) into η_{mech}, a single mechanical efficiency, and it has already been applied in expander models for organic Rankine cycles [14], [15]. With this model, the two variables that are used to design the compressor are its built-in volume ratio r_{v} (i.e. the ratio between intake and discharge chambers volumes) and its swept volume V_{s}. The compressor speed can vary between 2000 and 5000 rpm, depending on the operating conditions and to ensure that the model remains valid.

Afterwards, the fluid is condensed and sub-cooled in the high-pressure HEX, where heat is transferred to charge the thermal storage. The condensing temperature $T_{\mathrm{hp,cd}}$ is imposed as a design variable. The pressure losses $\Delta p_{\mathrm{hp,cd}}$ are also taken into account. The condenser exit temperature is obtained with the degree of sub-cooling $\Delta T_{\mathrm{hp,cd,sc}}$, which is also a design variable (see below for further details).

The fluid is finally expanded in a valve, and the expansion is modelled as adiabatic. The evaporation temperature in the low-pressure HEX is defined as the minimum between the cold cooling water temperature minus the pinch-point and the fluid temperature at the exit of the evaporator minus the desired degree of super-heating $\Delta T_{\mathrm{hp,ev,sh}}$.

The working fluid selected here is R1233zd(E). This choice is motived by the excellent performance it has shown in thermally integrated Carnot batteries [16], [17] and based on preliminary optimisation results.

The resistive heater is intended to be used as a peak unit due to its lower electricity to heat conversion ratio. When the heat pump runs at full load, extra power can be injected into the thermal storage with this component. The latter is modelled with an efficiency of 100%, meaning that all the electrical power is converted into heat [18]. Its maximal power is a design variable.

Sensible heat thermal storage. The sensible heat storage system is based on two water tanks, with different temperature levels. Water is adopted as storage material as it offers a high thermal storage density (i.e. up to 50 $\mathrm{kWh_{th}/m^3}$ [4]) at a low cost, in the considered temperature range (i.e. < 100 °C, see later). Although this configuration is more expensive than a single tank option, it avoids temperature uniformization within the tank due to the thermocline and temperature variations with the state of charge. Latent heat storage is not considered in this work as it is currently costly (i.e. 10-50 $/kWh compared to 0.1-10 $/kWh for sensible heat [4]). The tanks volume is selected as a design variable associated with the storage capacity.

The storage high temperature is set by the HP condensing temperature $T_{\mathrm{hp,cd}}$ and the pinch-point. The storage low temperature is set by the heat pump condenser exit temperature (i.e. thus the sub-cooling $\Delta T_{\mathrm{hp,cd,sc}}$) and by the pinch-point. Using these definitions, the storage temperatures remain constant over the year. In this model, the storage heat losses are neglected, assuming a sufficient thermal insulation (i.e. less than 0.5% loss per day [19]) and as the target application is for overnight storage (i.e. coupling with PV). This simplification is introduced to reduce the model complexity and was also used in other studies [11], sometimes operating at way higher storage temperatures than in the present case (i.e. up to 750 °C) [19].

Discharging system: heat engine. The heat engine (HE) is based on an organic Rankine cycle (ORC). Its evaporator extracts heat from the thermal storage while its condenser uses the cold cooling water as heat sink. The latter is chilled by the existing dry cooler, since it has been largely oversized for the current needs of the data centre. Based on the estimated remaining cooling capacity, it is decided that up to 800 kW can be rejected by the ORC condenser through it.

Like the HP, the HE is modelled with its thermodynamic cycle. After condensing, the fluid is sub-cooled in the low-pressure HEX where it rejects heat to the dry-cooled water. Its exit temperature is defined with the cold cooling water temperature and the pinch-point. The condensing temperature is obtained with degree of sub-cooling $\Delta T_{\mathrm{he,cd,sc}}$.
The fluid pressure is then increased in a feed pump, which is represented with the constant internal efficiency model:

$$w_{\mathrm{pump}} = \frac{\int_{\mathrm{su}}^{\mathrm{ex}} v\mathrm{d}p}{\eta_{\mathrm{pump}}} \simeq \frac{v_{\mathrm{su}}(p_{\mathrm{ex}} - p_{\mathrm{su}})}{\eta_{\mathrm{pump}}}. \tag{2}$$

Afterwards, the fluid evaporates and is super-heated in the high-pressure HEX. The evaporating temperature is obtained from the storage temperatures, the pinch-point and the desired degree of super-heating $\Delta T_{\mathrm{he,ev,sh}}$. The pressure losses $\Delta p_{\mathrm{he,ev}}$ are again taken into account.
The fluid is finally expanded in a volumetric expander. The latter is also represented with a simplified version of the semi-empirical model proposed and validated by Lemort [13]. This model has been used multiple times for design optimisation in ORCs [14], [15]. The expander speed can also vary between 2000 and 5000 rpm. Its swept volume and volume ratio are the design variables. The ORC working fluid is also R1233zd(E), for the same motivations as mentioned above.

Photovoltaic array. The PV array is modelled with `PVlib`, an experimentally validated open-source Python package [20], [21]. The PV current and voltage are evaluated with the single-diode model:

$$I_{\mathrm{PV}} = I_L - I_0 \left(exp\left(\frac{U + IR_{\mathrm{s}}}{n_{\mathrm{diode}} N_{\mathrm{s}} U_{\mathrm{th}}} \right) - 1 \right) - \frac{U + IR_{\mathrm{s}}}{R_{\mathrm{sh}}}. \tag{3}$$

The parameters in Eq. (3) are determined with the method developed by De Soto *et al.* [22], based on manufacturer data adopted from a typical monocrystalline silicon PV panel (Sun-power SPR X-19-240-BLK [23]). In this work, the nominal PV capacity to be installed is a design variable.

Auxiliary systems. Other auxiliaries are not represented in this model. It is assumed that their impact on the techno-economic performance can be neglected in a first step [7], [11].

Climate and system data

In this work, Louvain-la-Neuve (Belgium) is the considered location. The climate data (ambient temperature T_{ambient} and solar irradiance G) have been obtained with Renewables.ninja [24], [25] and correspond to the year 2019. The data centre related data (cooling water flow rate $\dot{m}_{\text{cooling}}$ and temperature $T^{\text{hot}}_{\text{cooling}}$, as well as servers consumption P_{servers}) have been gratefully provided by Center for High Performance Computing and Mass Storage from UCLouvain. The chiller power consumption has been synthetized with the method introduced above. All these data are depicted in Fig. A2, in *APPENDICES*.

Design variables and optimisation criteria

The nine independent design variables that were introduced above are: the volume ratios and swept volumes of the HP compressor and HE expander, the volume of each storage tank V_{tank}, the HP condensing and sub-cooling temperatures, the RH maximum power and the PV capacity. The design space associated with these variables is provided in Tab. 1. Note that the optimiser can exclude some components whenever beneficial (i.e. design value set to 0).

The PV maximum capacity was determined based on the available area around the data centre. The HP condensing temperature is limited by technological constraints on the compressor (i.e. lubrication oil, pressure ratio). The volume ratio range for the volumetric compressor and expander corresponds to commercially available technologies. Their maximum swept volumes can be considered as theoretically unconstrained since multiple components can be used in parallel.

Table 1. The design space associated with the design variables.

Parameter	Description	Units	Min	Max	Constraint type
$r_{\text{v,comp}}$	compressor volume ratio	$[-]$	1.5	5.0	technological
$V_{\text{s,comp}}$	compressor swept volume	$[cm^3]$	0	10,000	arbitrary
$r_{\text{v,exp}}$	expander volume ratio	$[-]$	1.5	5.0	technological
$V_{\text{s,exp}}$	expander swept volume	$[cm^3]$	0	10,000	arbitrary
V_{tank}	volume of a single tank	$[m^3]$	0	1000	arbitrary
$\Delta T_{\text{hp,cd,sc}}$	sub-cooling degree in HP	$[°C]$	0	70	physical
$T_{\text{hp,cd}}$	condensing temp. in HP	$[°C]$	25	100	technological
P_{RH}	resistive heater power	$[kW]$	0	800	arbitrary
P_{PV}	PV array nominal power	$[kW]$	0	800	physical

The Levelized Cost Of Electricity (LCOE) and Self-Sufficiency Ratio (SSR) are selected as design objectives for the optimisation. The LCOE is a techno-economic performance indicator and the SSR illustrates the resilience against large electricity price variations. They can be defined as:

$$\mathrm{LCOE} = \frac{\mathrm{CAPEX} + \sum_{t=1}^{\mathrm{LT}} \frac{\mathrm{OPEX}(t) + c_{\mathrm{el}}(t) E_{\mathrm{grid}}}{(1+r)^t}}{\sum_{t=1}^{\mathrm{LT}} \frac{E_{\mathrm{DC}}}{(1+r)^t}} \ , \tag{4}$$

$$\mathrm{SSR} = 1 - \frac{E_{\mathrm{grid}}}{E_{\mathrm{DC}}} \ , \tag{5}$$

where E_{DC} and E_{grid} are the annual electricity consumed by the data centre and provided by the grid respectively. $c_{\mathrm{el}}(t)$ is the average price of electricity for a given year, LT the system lifetime and r the discount rate. Note that in this LCOE definition, excess PV generation that is returned to the grid is sold at a zero price. This is a conservative choice, yet it favours the storage of electricity.

Economic model

CAPEX has five contributions in this model: $\mathrm{CAPEX_{HP}}$, $\mathrm{CAPEX_{RH}}$, $\mathrm{CAPEX_{ST}}$, $\mathrm{CAPEX_{HE}}$ and $\mathrm{CAPEX_{PV}}$. $\mathrm{CAPEX_{HP}}$ is evaluated with the correlation proposed by Croteau *et* Gosselin [26], which is expressed in $\mathrm{CAD_{14}}$. It is converted in $\mathrm{EUR_{14}}$ using a CAD/EUR rate of 0.6826 (average value for 2014 from European Central Bank). It is actualized in $\mathrm{EUR_{2020}}$ using the Chemical Engineering Plant Cost Index (CEPCI) [27]:

$$\mathrm{EUR_{2020}} = \frac{\mathrm{CEPCI_{2020}}}{\mathrm{CEPCI_{2014}}} \mathrm{EUR_{2014}} \ , \tag{6}$$

with $\mathrm{CEPCI_{2014}} = 576.1$ and $\mathrm{CEPCI_{2020}} = 596.2$. This method was used by other scholars [7], [11], [28]. $\mathrm{CAPEX_{ST}}$ is derived from the correlation for bullet pressure vessels constructed by Shamoushaki *et al.* [29] (expressed in $\mathrm{USD_{2020}}$). The USD/EUR rate is 0.8460 (average value for 2020). Other CAPEX parameters are given in Tab. A1, in *APPENDICES*.
In this model, the OPEX is evaluated as a fraction of the CAPEX, as often done in the literature [7], [11], [19]. Still, this definition is imperfect as the operational costs should be a function of the operations. Future works should therefore focus on improving the OPEX model for Carnot batteries.
The price of electricity is finally modelled as linear function of time:

$$c_{\mathrm{el}}(t) = (a_{\mathrm{el}} \cdot t + b_{\mathrm{el}}) \cdot (1 + \varepsilon_{\mathrm{el}}) \ , \tag{7}$$

where a_{el} is the average annual growth of the electricity price and b_{el} is the average price of electricity when commissioning the Carnot battery. $\varepsilon_{\mathrm{el}}$ is used to represent the uncertainty. These coefficients are fitted based on the Band IB prices of electricity for non-household consumers in Belgium from 2007 to 2021, extracted from the Eurostat database [30].

Optimisation method and global sensitivity analysis

Optimisation algorithm. In this work, the multi-criteria optimisation is carried out with the Nondominated Sorting Genetic Algorithm (NSGA-II) [31] through the framework developed by Coppitters *et al.* [32]. This metaheuristic algorithm is selected because of the complexity and non-linearity of the system. Further details on the method can be found in [32].

Uncertainty characterisation. The mean, standard deviation and distribution associated with each model parameter are provided in in Tab. A1, in *APPENDICES*.

The efficiencies of the compressor, expander and pump, as well as the pressure losses in HEX, can vary as the performance of the actual components cannot be known in advance. Looking at the sub-cooling and super-heating temperatures, they are set deterministic since they are typically used to control the system, although there is a small uncertainty in the measurement. On its side, the pinch-point is a function of the HEX performance, so it is set stochastic. The deviation in data centre power consumption and cooling water flow rate is the same, as both parameters are directly related to each other. The uncertainty on economic correlations is set based on their fitting error. The rather pessimistic lifetime prediction (i.e. 20 years compared to 25 years proposed in the literature [7], [11]) is constrained by the typical PV lifetime and expected data centre lifetime.
Note that the standard deviation set to each parameter should be discussed with regard to its impact on the global uncertainty of the parameter of interest.

Uncertainty quantification. In this work, uncertainty quantification is done by non-intrusive Polynomial Chaos Expansion (PCE) using the framework developed by Coppitters *et al.* [32]. Compared to conventional Monte Carlo simulations, as carried-out by McTigue *et al.* [19] for a CB based on the Brayton cycle, PCE achieves accurate statistics in less computational time.

PCE enables to characterize a surrogate model of the real model. This surrogate model is based on a set of orthogonal polynomials and corresponding coefficients that are tuned through evaluations of the real model. After quantifying the coefficients, Sobol' indices can be retrieved with analytical post-processing. These indices are used to assess the contribution of each uncertain parameter to the global variance of the selected objective. More details can be found in [32].

RESULTS AND DISCUSSION

In this section, design optimisation is first conducted to maximise the SSR and minimise the LCOE. This optimisation is followed by a sensitivity analysis of the obtained designs to quantify the distribution of their LCOE. To illustrate how the LCOE variation could be further reduced, the parameters contributing most to this variation are then highlighted through uncertainty quantification. The LCOS of the CB is finally introduced for comparison with other CB concepts.

Multi-criteria design optimisation

Based on the annual climate and demand data, multi-criteria deterministic optimisation has been conducted with NSGA-II to maximise the data centre SSR and minimise its LCOE. The clear conflicting nature of these objectives is illustrated by the Pareto front in Fig. 2: the LCOE increases exponentially with the SSR. The corresponding design variables are depicted in the left-hand side of Fig. 3.
The HP condensing temperature is not represented in Fig. 3 as it is 100 °C in all cases (the maximum allowed). This suggests that it is always more favourable to maximise the HE efficiency than the HP coefficient of performance (i.e. a higher storage temperature increases the HE efficiency while it reduces the COP of the HP). This result is a new contribution to the literature, and it is probably valid for very low temperature heat sources only (e.g. 24 °C), as it is in contradiction with the trends observed by Dumont and Lemort [17]. Further investigation should be conducted to assess the threshold of the heat source temperature above (resp. below) which it is more favourable to maximise the HP (resp. HE) performance.

From the results depicted in Fig. 2 & 3, three different system layouts can be distinguished. The first one includes PV but no storage (yellow curve). When the maximum PV capacity is deployed

(i.e. 800 kW), the second layout starts to involve storage to increase the SSR, but the Carnot battery is only charged with a RH (red curve). The last 4% in SSR are gained by using the HP (blue curve). The shaded band was obtained with uncertainty quantification and represents the uncertainty on the LCOE.

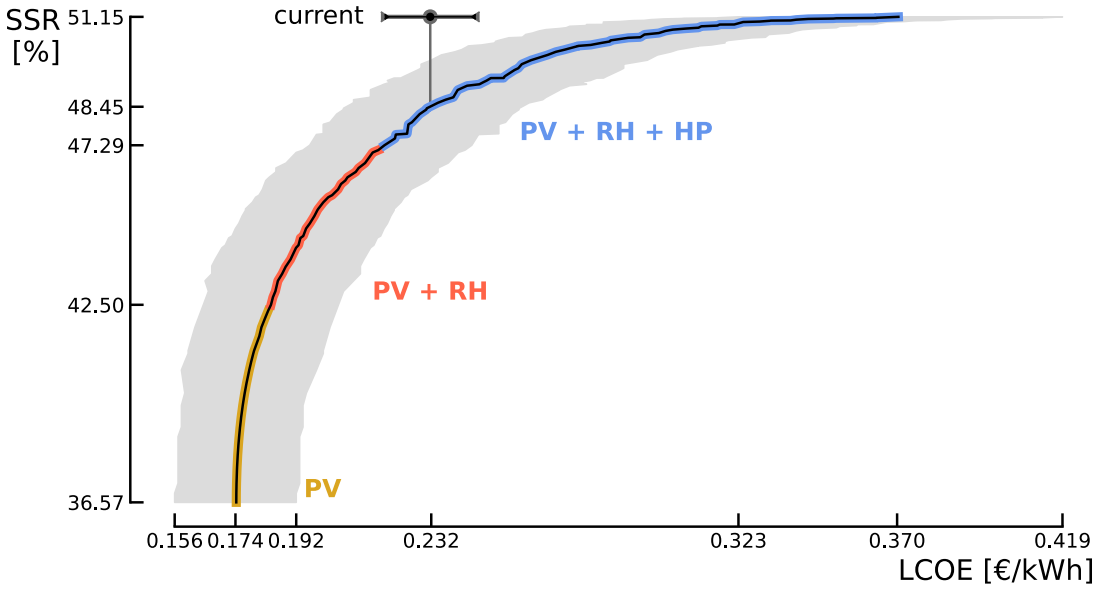

Figure 2. The Pareto front between the optimisation criteria. The shaded band indicates the uncertainty on the LCOE. The uncertainty on the LCOE for the current data centre is also depicted. Both uncertainties are represented with a 95% confidence interval.

These results indicate that, to increase the SSR in this scenario, it is preferable to deploy storage with a RH first. Despite its lower efficiency (i.e. $\eta_{\mathrm{CB}} \simeq 8\%$), it offers a lower cost (i.e. LCOE $\simeq 0.184€/\mathrm{kWh}$). If the aim is to further increase the SSR, the required higher efficiency (i.e. $\eta_{\mathrm{CB}} \simeq 12\%$) is achieved with the HP, but it is associated with a higher cost (i.e. $\mathrm{LCOE} = 0.218€/\mathrm{kWh}$). This result is a consequence of the fact that, since electricity is returned to the grid for free, not consuming it is equivalent to losing it, and it is therefore more attractive to store it at low cost despite the lower efficiency.
The estimated LCOE for the current data centre (i.e. without PV and CB) is also represented with a black dot in Fig. 2. Its uniform distribution is delimited with the inner-pointing black arrows. It is only shown for comparison with the LCOE including PV and CB, as the corresponding SSR is actually zero. Its location clearly shows that the system could reach a SSR of 48.5% while being economically competitive with the current data centre layout.

Some Key Performance Indicators (KPI) are also represented in the right-hand side of Fig. 3. These are (from top to bottom): the CB electrical efficiency η_{CB}, the HP coefficient of performance $\mathrm{COP}_{\mathrm{HP}}$, the HE efficiency η_{HE}, the LCOS and the fraction of E_{DC} that is actually coming from the storage. The LCOS is defined here by excluding the PV and electricity costs in the LCOE definition, and with the electricity produced by the HE at the denominator.
All the relations between the design variables and KPIs are consistent. It can for instance be observed that $\mathrm{COP}_{\mathrm{HP}}$ decreases with $\Delta T_{\mathrm{hp,cd,sc}}$ while η_{HE} increases with it. In fact, when $\Delta T_{\mathrm{hp,cd,sc}}$ decreases, the storage low temperature gets closer to the storage high temperature. Consequently, the $T_{\mathrm{he,ev}}$ increases and therefore η_{HE} as well. At the same time, the average pressure ratio seen by the ORC expander also increases, and $r_{\mathrm{v,exp}}$ therefore increases accordingly. Note that, in these results, convergence is not perfectly reached for $r_{\mathrm{v,exp}}$ (even though there is a net increasing trend),

despite the large population size (i.e. 126) and important number of generations (i.e. 275) used in NSGA-II. This can be explained by the wide range of pressure ratios over the year in the HE due to seasonal and design variations (i.e. from about 3 to 12), and by the moderate impact of this parameter on the SSR and LCOE compared to other design variables (i.e. PV power, tanks volume).

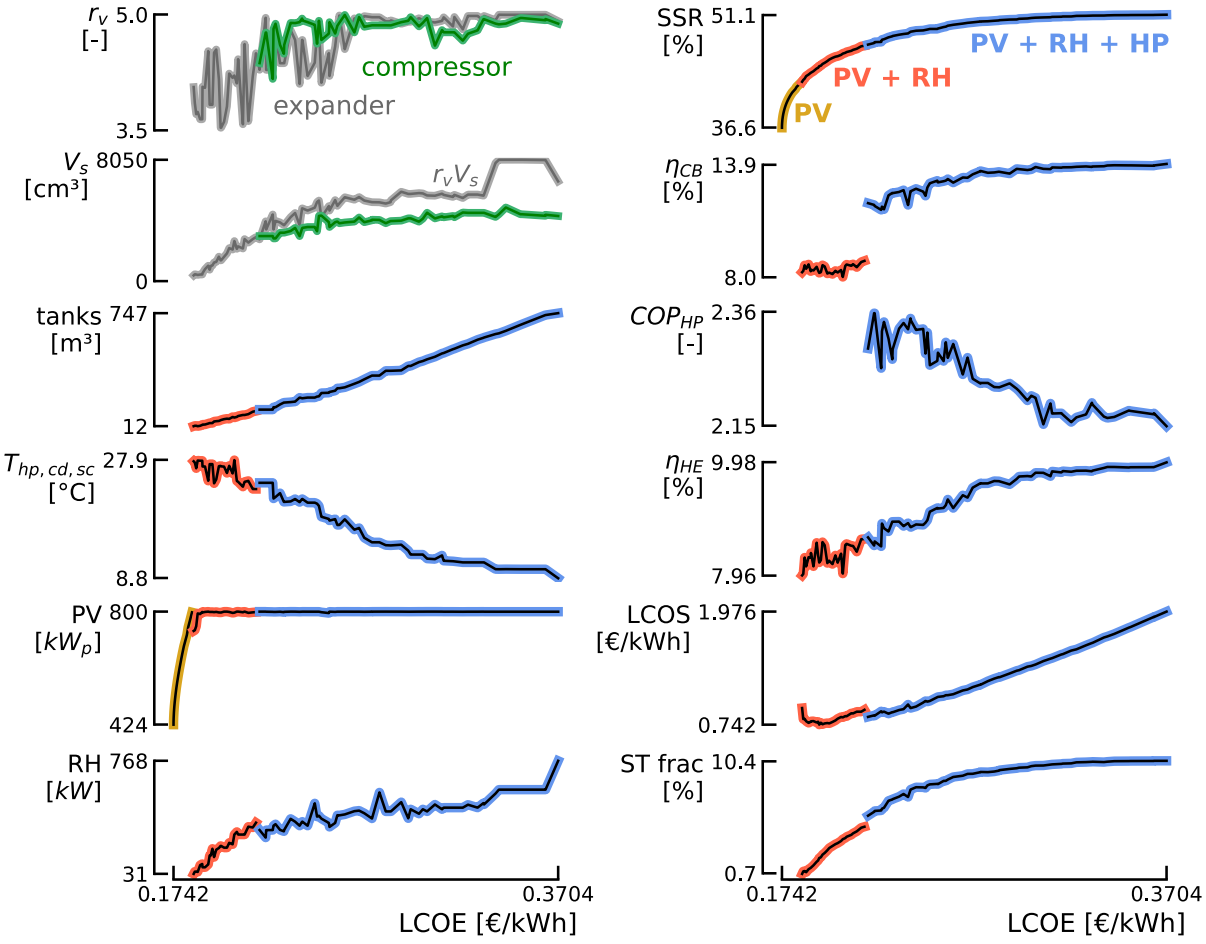

Figure 3. The designs variables and some KPI's after optimisation.

The SSR is limited to 51.1% as the maximum PV capacity (i.e. 800 kW) and ORC thermal power output (i.e. 800 kW) are reached.

Uncertainty quantification and global sensitivity analysis

The Sobol' indices corresponding to all uncertain parameters are evaluated to conduct the global sensitivity analysis. In a way, these indices illustrate the contribution of each parameter on a given quantity of interest: the closer they are to one, the greater the contribution of the parameter.

In Fig. 4, the Sobol' indices of the dominant parameters are depicted. For the designs in which few or no storage is installed (i.e. low LCOE), the uncertainty is mainly due to the electricity price and PV cost. As storage gets deployed (i.e. increasing LCOE), the effect of the electricity price and PV cost decreases whereas the system OPEX, servers power, HE price and tank price, start to have a stronger effect on the LCOE deviation. These results clearly indicate that restricting the uncertainty on the operational costs of the system would help to narrow the LCOE distribution. Efforts should also be made on reducing the uncertainty associated with the cost of the HE and storage system.

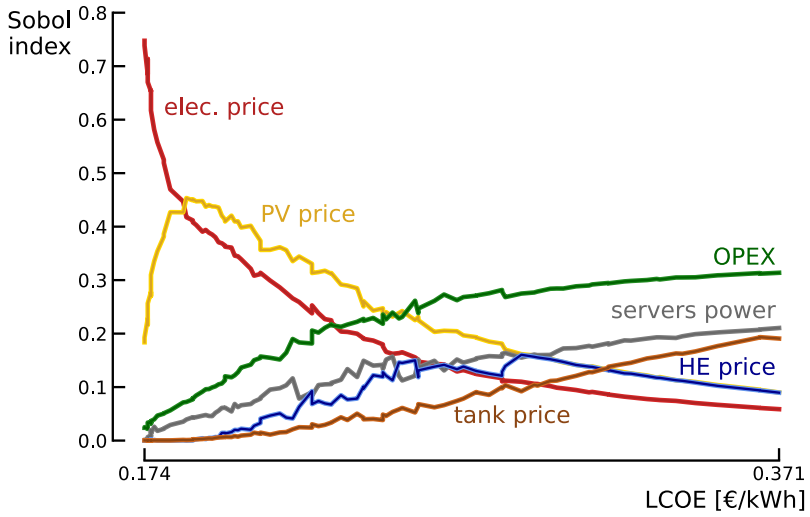

Figure 4. The Sobol' indices of the parameters driving the uncertainty on the LCOE.

Global sensitivity analyses have then been carried out to characterize the uncertainty on the LCOS of two Carnot battery designs (i.e. RH only and RH + HP). These designs have been chosen because of the low LCOE and low LCOS they provide. The results are depicted in Fig. 5.
It can first be observed that the LCOS distribution is very wide, especially compared to the standard deviations obtained by McTigue *et al.* [19]. This can be attributed to the larger distributions characterizing the capital costs and to the more important number of uncertainties in this work. Also note that the average LCOS for both designs is notably higher (i.e. from about two to five more times) than predictions published in the literature [7], [11]. This can be explained by the effect of operational constraints that are considered in this work (i.e. compared to ideal daily charge and discharge cycles), the use of different economic correlations and probably scale effects. The lower lifetime (i.e. 20 years compared to 25) also penalises the LCOS.

Sobol' indices in Fig. 5 indicate that the CB design based on the RH only is mainly sensitive to the RH and HE costs, to the OPEX and to a lesser extent to the storage cost. On the other hand, the design based on the RH + HP is more sensitive to the OPEX and HE cost.

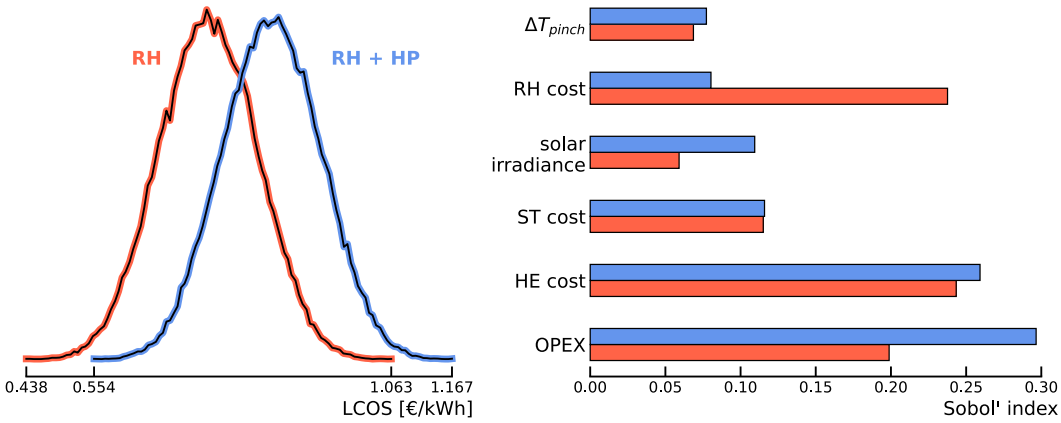

Figure 5. Global sensitivity analysis of the LCOS. *Left:* probability densities. *Right:* the Sobol' indices for: the pinch point, the solar irradiance, the RH cost, the storage system cost (i.e. the tanks), the operational costs and finally the HE cost.

CONCLUSION

This work investigates the techno-economic potential of integrating a Carnot battery based on a resistive heater, a heat pump and an organic Rankine cycle into a real 100 kW data centre, which is supported by a photovoltaic array. Its specificity is to take into account the operational constraints through annual simulations with an hourly resolution, as well as to consider techno-economic uncertainties on 20 model parameters. Using multi-criteria optimisation, the Carnot battery and PV array are designed to maximise the Self-Sufficiency Ratio of the data centre while minimising its Levelized Cost Of Electricity.

The results indicate that, adopting an integrated and systemic approach, minimising the LCOE does not imply maximising the storage efficiency. Instead, it is shown that, in the present case, degrading the storage efficiency can be afforded as it reduces the LCOE by saving part of the PV production, which would otherwise be lost to the grid. The best design trade-off suggests that, when deploying 800 kW of PV (i.e. maximum capacity), the SSR can reach 48.5%, of which 6% is gained from the Carnot battery. With this design, the expected LCOE is similar to that of the current data centre.

The global sensitivity analysis reveals that the uncertainty on the LCOE for the designs without storage is driven by the electricity price and PV cost, while for designs incorporating the CB, the uncertainty is dominated by the operational costs, the power consumption of the servers, and by the cost of the HE and the tanks. Further investigation of the storage cost also show that, considering the operational constraints, the obtained LCOS is relatively higher than values reported in the literature. Moreover, its wide distribution is due to uncertainties on the operational and capital costs of the Carnot battery.

Future work will focus on improving the performance of the system by exploring regeneration for the organic Rankine cycle (i.e. the expander outlet temperature ranges between 45 and 75 °C) and by considering new power management strategies. Other renewable sources of electricity, such as wind turbines, could be investigated as they are complementary to PV. The COP of the heat pump could also be increased by directly using the hot air (30 °C) trapped in the aisle as the heat source.

ACKNOWLEDGMENTS

Computational resources have been provided by the Consortium des Équipements de Calcul Intensif (CÉCI), funded by the Fonds de la Recherche Scientifique de Belgique (F.R.S.-FNRS) under Grant No. 2.5020.11 and by the Walloon Region.

Annual data corresponding to the data centre have been gratefully provided by the Center for High Performance Computing and Mass Storage from UCLouvain.

NOMENCLATURE

c_{el}	Cost of electricity	$[€/Wh]$
CAPEX	Capital expenditures	[€]
E	Electrical energy	$[Wh]$
G	Solar irradiance	$[W/m^2]$
LT	Lifetime	$[year]$
$\dot{m}$	Mass flow rate	$[kg/s]$
OPEX	Operational expenditures	[€]
Δp	Pressure losses	$[bar]$
p	Pressure	$[bar]$
P	Electrical power	$[W]$
Q	Thermal power	$[W]$
r_{v}	Built-in volume ratio	$[-]$
r	Discount rate	[%]

ΔT_{pinch}	Pinch-point	$[°C]$
$T_{\text{cooling}}^{\text{hot}}$	Hot cooling water temperature	$[°C]$
T	Temperature	$[°C]$
V_s	Swept volume	$[cm^3]$
V	Volume	$[m^3]$
w	Specific work	$[W/kg]$

Greek symbols

η	Efficiency	[%]

Sub- and superscripts

Carnot	Ideal Carnot cycle	he	Heat engine
comp	Compressor	hp	Heat pump
cooling	Cooling water	mech	Mechanical
cd	Condenser	sc	Sub-cooling
el	Electrical	sh	Super-heating
ev	Evaporator	su	Supply
ex	Exhaust	th	Thermal
exp	Expander		

Acronyms

CB	Carnot Battery	
COP	Coefficient Of Performance	$[-]$
EES	Electrical Energy Storage	
HE	Heat Engine	
HEX	Heat Exchanger	
HP	Heat Pump	
KPI	Key Performance Indicator	
LCOE	Levelized Cost Of Electricity	$[€/kWh]$
LCOS	Levelized Cost Of Storage	$[€/kWh]$
PCE	Polynomial Chaos Expansion	
PV	Photovoltaic	
RH	Resistive Heater	
SSR	Self-Sufficiency Ratio	[%]

APPENDICES

Detailed power management strategy

The power management strategy that has been used to simulate at each hour of the year the integration of the Carnot battery in the data centre is illustrated in Fig. A1.

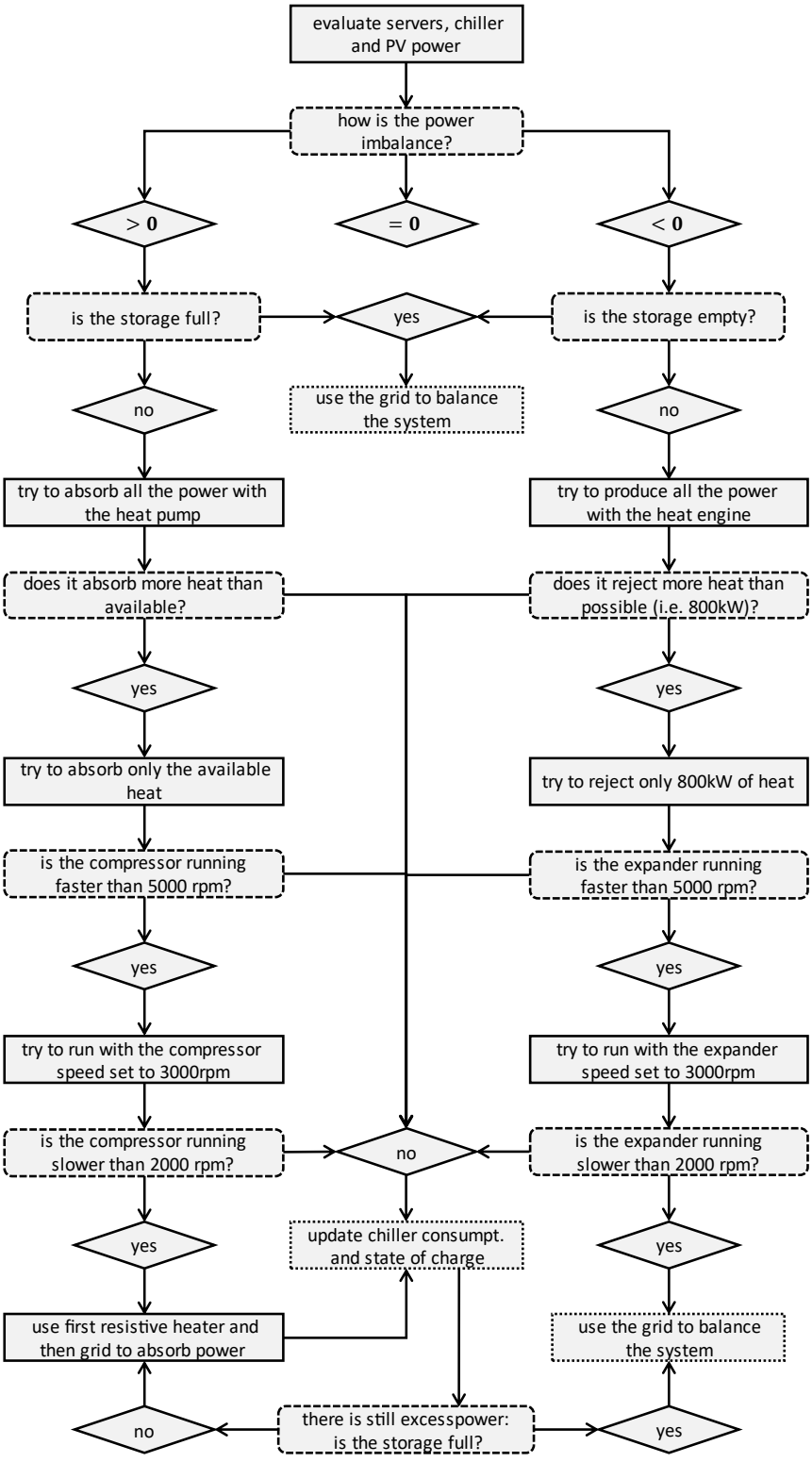

Figure A1. Power management strategy used to evaluate the system at each hour of the year.

Climate and system data

The annual data introduced in *Climate and system data* are represented in Fig. A2.

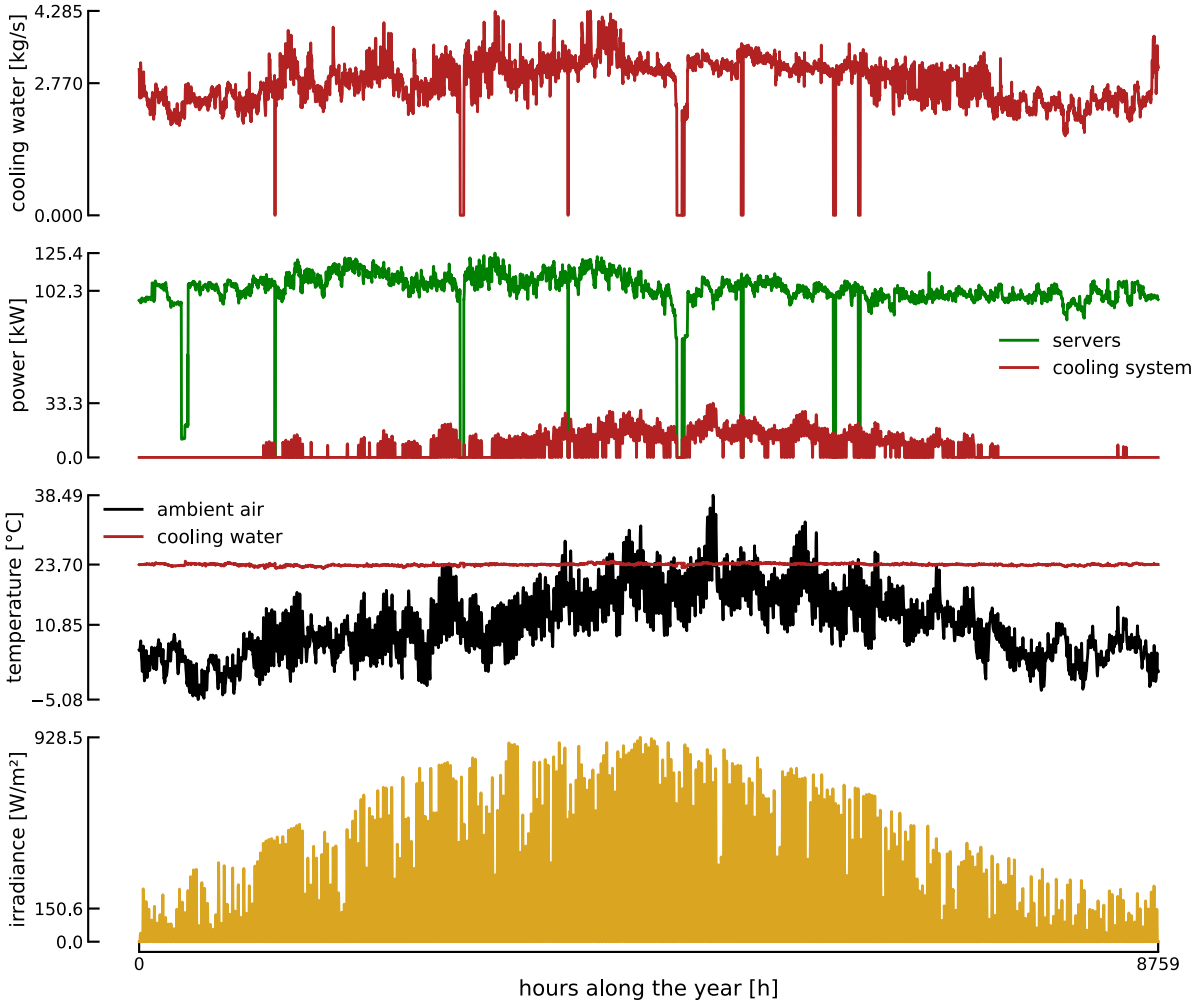

Figure A2. The hourly cooling water mass flow rate, servers and chiller electrical power consumptions, ambient and cooling water temperatures, and solar irradiance profiles for the UCLouvain data centre.

Uncertainty characterization

The deterministic and stochastic value of each model parameter is provided in Tab. A1.

Table A1. Uncertainty characterization of the model parameters.

Parameter	Units	Mean	Standard deviation	Distribution	Ref.
$\eta_{\text{mech,comp}}$	$[\%]$	72.5	2.5	uniform	[17], [33]
$\eta_{\text{mech,exp}}$	$[\%]$	72.5	2.5	uniform	[17], [33]
η_{pump}	$[\%]$	55	10	uniform	[17]
ΔT_{pinch}	$[°C]$	3.0	1.0	uniform	[7], [17]
$\Delta T_{\text{hp,ev,sh}}$	$[°C]$	4.0	0.0	n.a.	[7], [17]
$\Delta T_{\text{he,ev,sh}}$	$[°C]$	4.0	0.0	n.a.	[7], [17]
$\Delta T_{\text{he,cd,sc}}$	$[°C]$	4.0	0.0	n.a.	[17]
$\Delta p_{\text{hp,ev}}$	$[mbar]$	50	50	uniform	[17]
$\Delta p_{\text{hp,cd}}$	$[mbar]$	50	50	uniform	[17]
$\Delta p_{\text{he,ev}}$	$[mbar]$	50	50	uniform	[17]
$\Delta p_{\text{he,cd}}$	$[mbar]$	50	50	uniform	[17]
P_{servers}	$[W]$	annual data	5%	Gaussian	n.a.
$\dot{m}_{\text{cooling}}$	$[kg/s]$	annual data			
$T_{\text{cooling}}^{\text{hot}}$	$[°C]$	annual data	0	n.a.	n.a.
$\eta_{\text{chiller}}^{\text{Carnot}}$	$[\%]$	45	5	uniform	[34]
G	$[\%]$	annual data	7.8	Gaussian	[35]
T_{ambient}	$[°C]$	annual data	0.4	Gaussian	[35]
CAPEX_{HP}	$[€]$	correlation	$17\%_{\text{CAPEX}}$	uniform	[26]
CAPEX_{HE}	$[€/kW]$	2845	$35\%_{\text{CAPEX}}$	uniform	[36]
CAPEX_{ST}	$[€]$	correlation	$12\%_{\text{CAPEX}}$	uniform	[29]
CAPEX_{PV}	$[€/kW_p]$	475	125	uniform	[35]
CAPEX_{RH}	$[€/kW]$	175	75	uniform	[18], [37]
OPEX_{tot}	$[\%_{\text{CAPEX}_{\text{tot}}}]$	2.0	1.0	uniform	[7], [11], [19]
LT	$[years]$	20	0	n.a.	[35]
r	$[\%]$	7	0	n.a.	[38], [39]
a_{el}	$[€/MWh/year]$	2.84	0	n.a.	[30]
b_{el}	$[€/MWh]$	196	0	n.a.	[30]
ε_{el}	$[\%]$	0	9.2	uniform	[30]

REFERENCES

[1] A. Olympios *et al.*, 'Progress and prospects of thermo-mechanical energy storage - A critical review', *Progress in Energy*, Jan. 2021, doi: 10.1088/2516-1083/abdbba.

[2] J. Ramsebner, R. Haas, A. Ajanovic, and M. Wietschel, 'The sector coupling concept: A critical review', *Wiley Interdisciplinary Reviews: Energy and Environment*, vol. 10, no. 4, p. e396, 2021.

[3] W.-D. Steinmann, D. Bauer, H. Jockenhöfer, and M. Johnson, 'Pumped thermal energy storage (PTES) as smart sector-coupling technology for heat and electricity', *Energy*, vol. 183, pp. 185–190, Sep. 2019, doi: 10.1016/j.energy.2019.06.058.

[4] O. Dumont, G. F. Frate, A. Pillai, S. Lecompte, M. De Paepe, and V. Lemort, 'Carnot battery technology: A state-of-the-art review', *The Journal of Energy Storage*, vol. 32, Sep. 2020, doi: 10.1016/j.est.2020.101756.

[5] G. F. Frate, L. Ferrari, and U. Desideri, 'Rankine Carnot Batteries with the Integration of Thermal Energy Sources: A Review', *Energies*, vol. 13, no. 18, Art. no. 18, Jan. 2020, doi: 10.3390/en13184766.

[6] V. Novotny, V. Basta, P. Smola, and J. Spale, 'Review of Carnot Battery Technology Commercial Development', *Energies*, vol. 15, no. 2, p. 647, Jan. 2022, doi: 10.3390/en15020647.

[7] S. Hu, Z. Yang, J. Li, and Y. Duan, 'Thermo-economic analysis of the pumped thermal energy storage with thermal integration in different application scenarios', *Energy Conversion and Management*, vol. 236, p. 114072, May 2021, doi: 10.1016/j.enconman.2021.114072.

[8] V. Dias, M. Pochet, F. Contino, and H. Jeanmart, 'Energy and economic costs of chemical storage', *Frontiers in Mechanical Engineering*, vol. 6, p. 21, 2020.

[9] M. D'Antoni, D. Romeli, and R. Fedrizzi, 'Techno-economic analysis of air-to-water heat rejection systems', presented at the Eurosun Conference, 2014.

[10] I. H. Bell, J. Wronski, S. Quoilin, and V. Lemort, 'Pure and pseudo-pure fluid thermophysical property evaluation and the open-source thermophysical property library CoolProp', *Industrial & engineering chemistry research*, vol. 53, no. 6, pp. 2498–2508, 2014.

[11] R. Fan and H. Xi, 'Energy, exergy, economic (3E) analysis, optimization and comparison of different Carnot battery systems for energy storage', *Energy Conversion and Management*, vol. 252, p. 115037, Jan. 2022, doi: 10.1016/j.enconman.2021.115037.

[12] G. F. Frate, L. Ferrari, and U. Desideri, 'Multi-criteria investigation of a pumped thermal electricity storage (PTES) system with thermal integration and sensible heat storage', *Energy Conversion and Management*, vol. 208, p. 112530, Mar. 2020, doi: 10.1016/j.enconman.2020.112530.

[13] V. Lemort, 'Contribution to the Characterization of Scroll Machines in Compressor and Expander Modes', University of Liège, Liège, 2008.

[14] S. Quoilin, S. Declaye, B. F. Tchanche, and V. Lemort, 'Thermo-economic optimization of waste heat recovery Organic Rankine Cycles', *Applied Thermal Engineering*, vol. 31, no. 14, pp. 2885–2893, Oct. 2011, doi: 10.1016/j.applthermaleng.2011.05.014.

[15] S. Lecompte, H. Huisseune, M. van den Broek, S. De Schampheleire, and M. De Paepe, 'Part load based thermo-economic optimization of the Organic Rankine Cycle (ORC) applied to a combined heat and power (CHP) system', *Applied Energy*, vol. 111, pp. 871–881, Nov. 2013, doi: 10.1016/j.apenergy.2013.06.043.

[16] B. Eppinger, L. Zigan, J. Karl, and S. Will, 'Pumped thermal energy storage with heat pump-ORC-systems: Comparison of latent and sensible thermal storages for various fluids', *Applied Energy*, vol. 280, p. 115940, Dec. 2020, doi: 10.1016/j.apenergy.2020.115940.

[17] O. Dumont and V. Lemort, ‘Mapping of performance of pumped thermal energy storage (Carnot battery) using waste heat recovery’, *Energy*, vol. 211, p. 118963, Nov. 2020, doi: 10.1016/j.energy.2020.118963.
[18] K.-K. Cao, A. N. Nitto, E. Sperber, and A. Thess, ‘Expanding the horizons of power-to-heat: Cost assessment for new space heating concepts with Wind Powered Thermal Energy Systems’, *Energy*, vol. 164, pp. 925–936, Dec. 2018, doi: 10.1016/j.energy.2018.08.173.
[19] J. D. McTigue, P. Farres-Antunez, K. S. J, C. N. Markides, and A. J. White, ‘Techno-economic analysis of recuperated Joule-Brayton pumped thermal energy storage’, *Energy Conversion and Management*, vol. 252, p. 115016, Jan. 2022, doi: 10.1016/j.enconman.2021.115016.
[20] W. F. Holmgren, C. W. Hansen, and M. A. Mikofski, ‘pvlib python: a python package for modeling solar energy systems’, *Journal of Open Source Software*, vol. 3, no. 29, p. 884, Sep. 2018, doi: 10.21105/joss.00884.
[21] T. Gurupira and A. J. Rix, ‘PV SIMULATION SOFTWARE COMPARISONS: PVSYST, NREL SAM AND PVLIB’, presented at the Conf.: SAUPEC, 2017.
[22] W. De Soto, S. A. Klein, and W. A. Beckman, ‘Improvement and validation of a model for photovoltaic array performance’, *Solar Energy*, vol. 80, no. 1, pp. 78–88, Jan. 2006, doi: 10.1016/j.solener.2005.06.010.
[23] SUNPOWER, ‘X-SERIES RESIDENTIAL SOLAR PANELS: SUPPLEMENTARY TECHNICAL SPECIFICATIONS’. Document No. 505915 Rev F/ US.
[24] S. Pfenninger and I. Staffell, ‘Long-term patterns of European PV output using 30 years of validated hourly reanalysis and satellite data’, *Energy*, vol. 114, pp. 1251–1265, Nov. 2016, doi: 10.1016/j.energy.2016.08.060.
[25] I. Staffell and S. Pfenninger, ‘Using bias-corrected reanalysis to simulate current and future wind power output’, *Energy*, vol. 114, pp. 1224–1239, Nov. 2016, doi: 10.1016/j.energy.2016.08.068.
[26] R. Croteau and L. Gosselin, ‘Correlations for cost of ground-source heat pumps and for the effect of temperature on their performance’, *International Journal of Energy Research*, vol. 39, no. 3, pp. 433–438, 2015, doi: 10.1002/er.3243.
[27] D. Mignard, ‘Correlating the chemical engineering plant cost index with macro-economic indicators’, *Chemical Engineering Research and Design*, vol. 92, no. 2, pp. 285–294, 2014.
[28] G. F. Frate, L. Ferrari, and U. Desideri, ‘Multi-Criteria Economic Analysis of a Pumped Thermal Electricity Storage (PTES) With Thermal Integration’, *Front. Energy Res.*, vol. 8, p. 53, Apr. 2020, doi: 10.3389/fenrg.2020.00053.
[29] M. Shamoushaki, P. H. Niknam, L. Talluri, G. Manfrida, and D. Fiaschi, ‘Development of Cost Correlations for the Economic Assessment of Power Plant Equipment’, *Energies*, vol. 14, no. 9, p. 2665, May 2021, doi: 10.3390/en14092665.
[30] Eurostat, ‘Electricity prices for non-household consumers - bi-annual data (from 2007 onwards)’. Eurostat, Apr. 22, 2022.
[31] K. Deb, A. Pratap, S. Agarwal, and T. Meyarivan, ‘A fast and elitist multiobjective genetic algorithm: NSGA-II’, *IEEE transactions on evolutionary computation*, vol. 6, no. 2, pp. 182–197, 2002.
[32] D. Coppitters, ‘Robust Design Optimization Of Hybrid Renewable Energy Systems’, Vrije Universiteit Brussel (VUB), University of Mons (UMONS), Mons, 2021.
[33] B. Eppinger, D. Steger, C. Regensburger, J. Karl, E. Schlücker, and S. Will, ‘Carnot battery: Simulation and design of a reversible heat pump-organic Rankine cycle pilot plant’, *Applied Energy*, vol. 288, p. 116650, Apr. 2021, doi: 10.1016/j.apenergy.2021.116650.

[34] I. Wyssen, L. Gasser, B. Wellig, and M. Meier, ‘Chiller with small temperature lift for efficient building cooling’, 2010, vol. 2010.
[35] D. Coppitters, W. De Paepe, and F. Contino, ‘Robust design optimization of a photovoltaic-battery-heat pump system with thermal storage under aleatory and epistemic uncertainty’, *Energy*, vol. 229, p. 120692, Aug. 2021, doi: 10.1016/j.energy.2021.120692.
[36] S. Lemmens, ‘Cost Engineering Techniques and Their Applicability for Cost Estimation of Organic Rankine Cycle Systems’, *Energies*, vol. 9, no. 7, p. 485, Jun. 2016, doi: 10.3390/en9070485.
[37] E. Styrelsen, ‘Technology data for energy plants—generation of electricity and district heating, energy storage and energy carrier generation and conversion’, *Energinet. dk, Energi Styrelsen, Denmark*, 2012.
[38] M. Petrollese and D. Cocco, ‘A multi-scenario approach for a robust design of solar-based ORC systems’, *Renewable Energy*, vol. 161, pp. 1184–1194, Dec. 2020, doi: 10.1016/j.renene.2020.07.120.
[39] A. Toffolo, A. Lazzaretto, G. Manente, and M. Paci, ‘A multi-criteria approach for the optimal selection of working fluid and design parameters in Organic Rankine Cycle systems’, *Applied Energy*, vol. 121, pp. 219–232, May 2014, doi: 10.1016/j.apenergy.2014.01.089.